 doi:10.20944/preprints202104.0612.v1

Article

Secure Air Traffic Control at the Hub of Multiplexing on the Centrifugo-Pneumatic Lab-on-a-Disc Platform

Jens Ducrée

School of Physical Sciences, Dublin City University, Glasnevin, Dublin 9, Ireland
Correspondence: jens.ducree@dcu.ie; Tel.: +353 (1) 700 5377

Abstract: Larger-scale integration (LSI) resides at the heart of comprehensive sample-to-answer automation and parallelisation of assay panels for frequent and ubiquitous bioanalytical testing in decentralised the point-of-use / point-of-care settings. With an emphasis on rotational, centrifugo-pneumatic flow control, this paper employs a virtual "digital twin" strategy, considering experimental tolerances, to efficiently design such "Lab-on-a-Disc" systems featuring high packing density, reliability, configurability, modularity, manufacturability, performance while minimizing development and fabrication cost.

Keywords: centrifugal microfluidics; Lab-on-a-Disc; centrifugo-pneumatic flow control; integration; multiplexing, parallelization, sample-to-answer; reliability; tolerances, design-for-manufacture; digital twin; event-triggering

Introduction

There is a strong market need for providing rather complex bioanalytical testing capabilities, that are currently carried out by well-trained personnel in professional facilities, for manifold decentralized use cases. Main applications are found in biomedical point-of-care and global diagnostics, liquid handling automation for the life sciences, process analytical techniques and cell line development for biopharma as well as monitoring the environment, infrastructure, industrial processes and agrifood. Since the early 1990s, microfluidic "Lab-on-a-Chip", also - quite synony-mously - referred to as Micro Total Analysis Systems ("μTAS") , have been proposed to cater for these strong demands [1].

Since these pioneering days, centrifugal microfluidic technologies have played a significant role in the scientific community [2-23], and, even more, in commercially directed initiatives [24-35]; as common in new technologies, many of these companies have filed significant success, while others were absorbed or discontinued in the meantime. The development of such "Lab-on-a-Disc" (LoaD) systems involves the well-coordinated development of fluidic, manufacturing, instrumentation, software, detection, and bioassay capabilities. The latter two elements of the LoaD technology stack are often closely derived from established reagent kits, and optical or electrochemical sensing techniques. However, the degrees of freedom for fluidic layouts are significantly restricted, chiefly owing to the typical, single-use character of the carrier chip as the multi-branched channel networks can typically not be regenerated.

To still mitigate the cost, the disposable chips are usually produced in polymer materials by (compression-)injection moulding that are well established in optical data storage manufacture, and thus predominantly adopt geometries like Compact Disc™ (CD), Digital Video Disc (DVD) or Blu-ray formats (or sections therefore) with their standard 12-cm diameter, thickness of about 1.2 mm, and a central, 15-mm diameter hole for coupling to the spindle. The disc shape is also commensurate with the rotational symmetry of the centrifugal field. While centrifugal microfluidic devices have been implemented on many shapes, e.g., circular segments, semicircle or standard (rectangular) microscope slide, for the sake of this work, the popular term "disc" will represent all types of chip formats attached to a rotor.

Preprints (www.preprints.org) | NOT PEER-REVIEWED | Posted: 22 April 2021 doi:10.20944/preprints202104.0612.v1

In a similar way as a CD player or discman, LoaD systems usually feature a modular setup with a rather rugged, possibly portable instrument taking up the fluidic carrier which is equipped with the spindle motor, control, detection, and display units. For immersion with most point-of-use scenarios, all (liquid or dry) reagents need to be (pre-)stored on the chip so that only the (bio-)sample needs to be loaded by the end user.

While the physical representation, i.e., pits and lands, on optical storage media are of micron- and sub-micron size, the channels and chamber in microfluidic systems commonly need to handle volumes in the upper microliter range, at least on the inlet side, corresponding to milli- to centimeter lateral dimensions. Such multi-scale manufacture of the low-aspect ratio discs imposes significant challenges on manufacturing and assembly, which need to be addressed separately for each fluidic design and fabrication technology. Furthermore, as other conventional Lab-on-a-Chip technologies, the development of LoaD applications goes through several stages, often starting from prototyping for initial proof-of-concept, pilot series, e.g., to establish sufficient statistics for fluidic and bioanalytical validation, and substantial optimization towards commercial mass production.

Each fabrication scheme along the scale-up, e.g., precision milling in prototyping and subsequent, tool-based replication, involves restrictions on geometries, manufacturing tolerances, artefacts, and often considerable efforts for setting up the process [36]. Typically, any change in the fluidic, materials, manufacturing processes, detection concepts, instrumentation, software, reagents, and assay protocol may induce mutual interference. Following, diligently following design-for-manufacture (DfM) guidelines and proper interface management are thus key for reaching high technology readiness levels (TRLs) within reasonable techno-economical boundary conditions.

Most centrifugal microfluidic platforms operate in a batch-wise "stop-and-go" fashion, meaning that Laboratory Unit Operations (LUOs) for sample preconditioning, like metering, aliquoting, removal of bioparticles, and resuspension of dry and mixing with liquid reagents are gated by normally closed valves. Upon completion of each LUO, the liquid is forwarded to the next step. Techniques for such valving can be broadly distinguished by their retention and release mechanisms [37].

Initial LoaD concepts were mainly based on siphoning [25, 26] and capillary burst valves [2] typically requiring precise definition of geometrical features or surface coatings. Concepts based on sacrificial materials, for instance, wax [38, 39], membranes [40] or stick-packaging [41], provide a liquid and vapor barrier, thus making them suitable for longer-term onboard storage of liquid reagents; yet, they either require an externally powered unit [42, 43] or high, often poorly defined release rates. Rudimentary centrifugo-pneumatic (CP) flow control mechanisms were introduced [44, 45], which tend to require large, rotationally induced pressure heads for opening, therefore making them primarily suitable for valving the penultimate LUO in a liquid handling sequence.

Subsequent work refined the release mechanism of these CP valving techniques with venting their compression chamber. Other than removing the seal by instrument-based such as lasers [40] or xurography [46], (water) dissolvable films (DFs) covering outlets that are pneumatically coupled to the compression chamber were opened by ancillary liquids [47]. With this strategy, complex, highly multiplexed networks offering "hand-shake" as well as logical flow control, such as AND, OR and IF conditionals, could be developed, which operate widely independent of the of the spin protocol [48-52].

Based on a digital twin concept factoring in experimental tolerances to deliver high predictability for batch-mode operated microfluidic LoaD platforms [37], this paper investigates key design features gearing centrifugo-pneumatically coupled valving networks towards large-scale integration (LSI) of parallelized, multi-step bioassay panels.

Basics of Rotational Flow Control

Centrifugal Field

According to classical mechanics, an object of (uniform) density ϱ_{part} and volume V with a centre of mass located at a distance R from the axis of rotation experiences a centrifugal field density

Preprints (www.preprints.org) | NOT PEER-REVIEWED | Posted: 22 April 2021 doi:10.20944/preprints202104.0612.v1

$$f_\omega = F_\omega / V = \varrho_{\text{part}} \cdot R \cdot \omega^2 \quad (1)$$

at the angular spin rate $\omega = 2\pi \cdot \nu$. Note that in typical microfluidic scenarios, a (bio-)particle suspended in a liquid of density ϱ experiences buoyancy, so the ϱ_{part} in f_ω (1) would refer to the difference between the densities $\varrho_\Delta = \varrho_{\text{part}} - \varrho$ of the object and its surrounding medium.

While not relevant the immediate context of this paper focusing on valving, the rotationally induced Coriolis (pseudo) force $|f_v| = 2\varrho \cdot \omega \cdot v$ acts on objects traveling at a speed $v = \omega \cdot r$ in the non-inertial frame spinning at ω. In common LoaD systems, $\vec{f_v}$ is directed opposite to the direction of motion in the plane of the disc, and has been used for agitating advective mixing [53, 54] and routing [55].

Pressure Contributions

Rather than forces, the response of liquids as continuous media to a field f_ω (1) are better captured by pressures $p = F/A$, i.e., force F per unit (cross-sectional) area A. In the context of the essentially hydrostatic approximation underlying the mainstay of this paper, a valve is represented by a geometrical structure Γ which is composed of chambers and interconnecting channels holding a liquid of total volume U_0. On LoaD systems, the distribution of the (contiguous) liquid $\Lambda(\omega)$ forms under the impact of the centrifugal pressure head

$$p_\omega = \varrho \cdot \bar{r}\Delta r \cdot \omega^2 \quad (2)$$

scaling with the square of the spin rate ω and the radial product

$$\bar{r}\Delta r = \frac{1}{2}(r^2 - r_0^2) \quad (3)$$

composed of its mean radial position

$$\bar{r} = \frac{1}{2}(r + r_0) \quad (4)$$

and its radial extension

$$\Delta r = r - r_0 \quad (5)$$

(radially) confined by its inner and outer menisci r_0 and r, respectively.
The net counterpressure in the axial z-direction opposing p_ω can be compounded to $p_z = p_\leftarrow - p_\rightarrow$ with (the gradients of) pressures directed parallel $p_\rightarrow$ and opposite $p_\leftarrow$ to the main (axial) direction of the channel. Based on the hydrostatic equilibrium

$$p_\omega + p_\rightarrow = p_\leftarrow \Leftrightarrow p_\omega = p_z \quad (6)$$

and the continuity of liquid volume

$$\frac{d}{dt}\int_\Lambda dV = 0 \quad (7)$$

the two (radial) positions r and r_0 of its confining menisci, and thus the distribution Λ throughout Γ, can hence be calculated.

The contributions $p_\rightarrow$ and $p_\leftarrow$ might be generated externally [56], e.g., by compressed air bottles, on-board pumps, or mechanical valves (corresponding to $p_\leftarrow \mapsto \infty$); for more common, rotationally controlled valving mainly investigated in the context of this work, pneumatic pressures

$$p_V = p_0 \cdot \frac{V_0}{V} \quad (8)$$

linked to the compression of a gas volume enclosed by the liquid from their original size V_0 at the atmospheric pressure $p_0 = 1013.25$ hPa (at standard conditions) to $V < V_0$, e.g., by mechanical work or temperature change, and capillary action

$$p_\Theta = \frac{4\sigma}{D} \cdot \cos\Theta \quad (9)$$

Preprints (www.preprints.org) | NOT PEER-REVIEWED | Posted: 22 April 2021 doi:10.20944/preprints202104.0612.v1

governed by the diameter D of the channel (with round cross section) and its contact angle Θ with a liquid of surface tension σ have been implemented.

Angular Acceleration

Certain LUOs, e.g., for mixing by chaotic advection [57] and or mechanical cell lysis [58] with obstacles or (magnetic) beads, benefit from rotational accelerations $dv/dt = R \cdot d\omega/dt$. Assuming a solid disc of mass m_{disc} and radius R_{disc}, and thus a moment of inertia $I_{\text{disc}} \approx 0.5 \cdot m_{\text{disc}} \cdot R_{\text{disc}}^2$ and resulting angular momentum $L_{\text{disc}} = I_{\text{disc}} \cdot \omega$, the steepness of the ramps $d\omega/dt = \tau_{\text{spindle}}/I_{\text{disc}}$ is limited by the maximum torque τ_{spindle} of the spindle motor. Such angular accelerations might be approximated by an inertially induced pressure term

$$p_m = \frac{\varrho \cdot U \cdot R \cdot d\omega/dt}{A} \leq \frac{\varrho \cdot U \cdot R \cdot \tau_{\text{spindle}}}{A \cdot I_{\text{disc}}} \tag{10}$$

for a fluid volume U of density ϱ traveling at a speed $v = R \cdot \omega$ at a radial position R through a channel of cross section A.

Note that LoaD systems feature cavities, i.e., channels and chambers, through which the liquids move along the assay protocol; the moment of inertia $I = I(t)$ thus increases over time t with the centrifugally outbound motion of (the centre of mass of the) the liquid distribution $\Lambda(t)$.

Critical Spin Rate

The common, normally-closed valves can be characterized by a first retention phase when the outer meniscus of Λ at r is retained upstream of a critical point in Γ. Subsequent, rotationally induced release of (part of) the liquid volume U_0 to an outlet is then prompted through shifting the spin protocol $\omega(t)$ across a critical frequency Ω. For spin-rate independent axial pressure heads $p_{\rightarrow}$ and $p_{\leftarrow}$, and thus also p_z, we derive a critical frequency

$$\Omega = \sqrt{\frac{p_{\leftarrow} - p_{\rightarrow}}{\varrho \cdot \bar{r}\Delta r}} = \sqrt{\frac{p_z}{\varrho \cdot \bar{r}\Delta r}} \tag{11}$$

by combining (2) and (6). High- and low-pass valves distinguish by whether the release is triggered by lifting or lowering ω across Ω (11), respectively.

Alternative to modulating $\omega(t)$, the hydrostatic equilibrium (6) may also be altered by adding a liquid volume V_Δ to one end of Λ for elevating Δr (and possibly also $\bar{r}$) in p_ω (2). Furthermore, in centrifugo-pneumatic valves delineated by $p_{\rightarrow} = p_0$ and $p_{\leftarrow} = p_V$ (8), the outer compression chamber may be enlarged or vented, i.e., $p_{\leftarrow} = p_V \mapsto p_0$, for triggering liquid release.

Note that for highly dynamic systems, inertial effects will have to be included in calculating the frequency Ω (11), e.g., by including an inertial pressure term $p_m > 0$ (10) in $p_{\rightarrow}$, which would thus lower the effective retention rate compared to the quasi-hydrostatic case mainly considered in the course of this work.

Siphon Valving

From the early days of LoaD systems, siphoning principles have been utilized for centrifugal flow control. In these geometries Γ, a (usually larger) inlet reservoir is connected by an outlet channel featuring inbound and outbound segments with an inner crest point R_{crest} to a receiving chamber. During retention, the outer meniscus r resides in the inbound segment where the centrifugal pressure p_ω (2) points antiparallel to the direction of p_z, thus effectively stabilizing the retention distribution $\Lambda(\Omega)$ against perturbations, such as inertial effects, and droplet break-off. This phase is characterized by a Δr (and $\bar{r}$) between the front meniscus in the inbound section r and the liquid level in the inlet reservoir r_0, so that $p_z(r) = p_\omega \propto \bar{r}\Delta r$ (3). The axial direction of p_z determines the sign of Δr, i.e., whether r is elevated or depressed with respect to r_0.

In many cases, siphons connect two vented (or very large) chambers, thus neutralizing the impact of p_0 applying at either end. In macroscopic setups, priming of the siphon channel is then triggered by addition of a sufficient volume V_Δ to the inlet for liquid to progress past the crest point

Preprints (www.preprints.org) | NOT PEER-REVIEWED | Posted: 22 April 2021 doi:10.20944/preprints202104.0612.v1

at R_{crest}. While such release mechanisms can also be deployed for miniaturized systems, LoaD technologies have resorted to priming by capillary action, i.e., $p_{\rightarrow} = p_{\Theta} \propto \cos\Theta$ (9), with a hydrophilically coated siphon outlet with $\Theta < 90°$. Furthermore, pneumatic pumping through compression of a volume in a side chamber connection to the inlet has been explored [59]. In both of these low-pass constructs, a continuous liquid "pulley" effect sets in once the condition $\Delta r > 0$ is met between the menisci in the inner reservoir and the outbound segment; at this stage, also p_{ω} (2) works in tandem with $p_z > 0$ to drag the liquid radially outwards, thus further increasing Δr in a self-amplifying pumping mechanism.

In centrifugo-pneumatic (CP) siphon valving, $p_{\rightarrow} = p_0$ and $p_{\leftarrow} = p_V$ (8), i.e., $p_z = p_0 \cdot (V_0/V - 1)$, so that $\Delta r > 0$ is needed to drive the liquid past the inner create point R_{crest} all the way to the outlet chamber against shrinking compression volume V, and thus growing $p_V \propto 1/V$ (8). Instead of a self-propelling pulley effect promoted by a narrow outlet, advancement of the outbound meniscus requires steady increase of the spin rate ω, and, as long as there is a positive $\Delta r > 0$, the centrifugal pressure $p_{\omega} \propto \Delta r \cdot \omega^2$ (2) can (at least mathematically) match any counteracting p_V (8).

For a sufficiently narrow outlet channel, the integrity of the liquid plug might be preserved by the surface tension σ all the way until the front meniscus reaches the entrance of the outer chamber at the radial position R_{cham}, after which liquid is transferred. However, for larger cross sections A of the outbound segment of the siphon and high spin rates, the liquid will creep or drip after passing the crest segment R_{crest} into the outer chamber until $\Delta r = 0$, rather than a showing a piston-like behavior. There are thus critical frequencies Ω and Ω^* (11) characterizing the retention and release into the outer chamber, which depend on whether the liquid plug is cut at R_{crest} or R_{cham}. In either case, a volume U_{loss} remains in the upstream part of the valve.

Note that the critical frequency Ω (11) of CP valves, i.e., their basic as well as their siphon variants, can be widely configured by the original compression volume V_{C}; its permanently gas-filled parts can be located at "anywhere", e.g., where disc real estate is still available, if the fractional volume compartments remain pneumatically interconnected.

Centrifugo-Pneumatic Siphon Valving with Dissolvable-Film Membranes

In order to supersede the prerequisite for external actuation of venting, CP valves have integrated with sacrificial, fluidically impermeable [60] membranes in their final receiving chamber; these seal the compression chamber until they get in contact with their solvent, usually an aqueous bioliquid. The opening of these dissolvable films (DFs) requires the transfer of sufficient liquid U_{DF} to raise the filling level above its location.

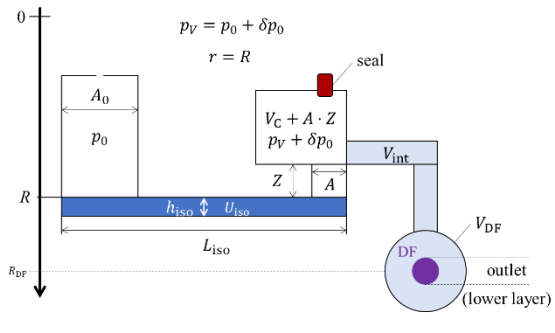

(a) Filling of isoradial channel with U_{iso} to isolate the compression chamber of volume $V_{\mathrm{C}} + A \cdot Z$ at p_0.

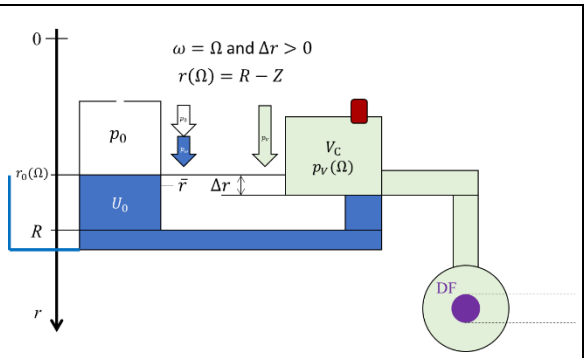

(b) Topping up the liquid to U_0 so that the front meniscus is placed at the crest point $R_{\mathrm{crest}} = R - Z$ while spinning at the critical frequency $\omega = \Omega$.

Preprints (www.preprints.org) | NOT PEER-REVIEWED | Posted: 22 April 2021 doi:10.20944/preprints202104.0612.v1

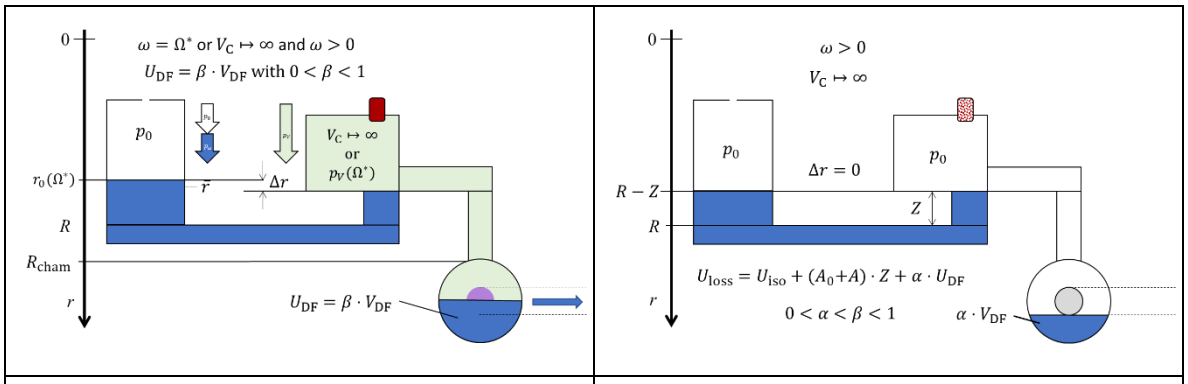

(c) A volume U_{DF} has arrived in the compression chamber to wet and open the DF.

(d) Residue (maximum) U_{loss} left in upstream and outer part of Γ after completion of liquid transfer.

Figure 1. CP-DF siphon valving. The measures of the default geometry Γ (linearized display) are compiled Table S1. The structure consists of an inlet reservoir of cross section $A_0 = d_0 \cdot w_0$ with depth w_0 and width w_0 which is connection through a (narrow) isoradial channel of volume $U_{iso} = d_{iso} \cdot L_{iso} \cdot h_{iso}$ positioned at R to a radially inbound section of cross section $A = d \cdot Z$ of depth d and radial extension Z. During retention, the outer part represents is gas-filled compression chamber, with a main compartment of volume $V_{C,0}$, isoradial and radial sections of volume V_{int} connecting to a round chamber centered at R_{DF}. This outer compartment of volume V_{DF} features a dissolvable-film (DF) membrane which intermittently covers a centrally placed vertical via leading to an outlet in a lower layer.

Performance Metrics

In this section, quantitative characteristics for rotationally controlled valving are specified that will be important towards functional LSI requiring high packing density paired with system-level reliability. These metrics are run along the example of for CP-DF siphon valving (**Figure 1**), but can be readily extended to further valve types.

High Field Strengths for LUOs

LUOs such as plasma separation become most efficient at high field strengths f_ω (1). Given a medium of (differential) density ϱ retained by a valve of critical spin rate Ω (11) in a reservoir at a position R, we obtain

$$\hat{f}_\omega = \varrho \cdot R \cdot \Omega^2 \tag{12}$$

for the maximum field strength available for the LUO. As shifting R in (12) mostly impacts $\bar{r}$ in the radial product $\bar{r}\Delta r$ (11), the primary parameter towards maximizing $\hat{f}_\omega$ (12) for a given retention rate $\omega \leq \Omega \propto 1/\sqrt{\bar{r}\Delta r}$ (11) is Δr, i.e., the liquid distribution $\Lambda(\Omega)$ which can be geared by the geometry Γ for a given U_0 and Ω. The dimensionless metric

$$\bar{f}_\omega = \frac{R}{R_{max}} \cdot \frac{\Omega^2}{\omega_{max}^2} \tag{13}$$

references $\hat{f}_\omega$ (12) to the largest available field strength at the maximum radial position R_{max} and (safe) rotational frequency ω_{max} that can be produced by the spindle motor.

Radial Space

Due to the unidirectional nature of the centrifugal field f_ω (1), the (centre of gravity) of a liquid distribution Λ must always advance in the radially outbound direction. At least in absence of externally energized centripetal pumping, subsequent LUOs must thus radially stagger their processing chambers.

Preprints (www.preprints.org) | NOT PEER-REVIEWED | Posted: 22 April 2021 doi:10.20944/preprints202104.0612.v1

As part of such serial arrangement, the unidirectional centrifugal field f_ω (1) puts a price tag on the radial position

$$\bar{R} = \frac{R_{\max} - R}{R_{\max} - R_{\min}} \tag{14}$$

echoing that a central placement is most favorable to keep sufficient room for downstream LUOs. Also, the overall consumption of radial space

$$\overline{\Delta R} = \frac{\hat{r} - \check{r}}{R_{\max} - R_{\min}} \tag{15}$$

with the inner and outer boundaries $\check{r}$ and $\hat{r}$ of the structure Γ, respectively, should be taxed towards optimization of packing density.

Spatial Footprint

The real estate available for patterning Γ on a discoid carrier is limited, e.g., between $R_{\min} = 7.5$ mm outside the 15-mm central hole and $R_{\max} = 5.5$ cm to leave an outer rim for bonding a lid, e.g., with a radial extension of 5 mm, for chip geometries derived from conventional optical storage formats. This makes central real estate, where the space is smallest, most precious, and the radial position $\bar{R}$ (14) most favorable, while limiting the maximum field strength $\hat{f}_\omega$ (12) for LUOs that can still be sustained by their downstream control valves.

If we consider a function of the full (azimuthal) width $W(r)$ of Γ along the radial direction r, a simple measure of the spatial footprint would be the entire surface area enclosed within its outer contours confined by $\check{r}$ and $\hat{r}$. Considering the scarcity of central space, we introduce the metric

$$\bar{A} = \frac{1}{R_{\max} - R_{\min}} \int_{R_{\min}}^{R_{\max}} \frac{W(r)}{2\pi \cdot r} dr \tag{16}$$

which relates the spatial footprint of Γ at R with respect to the total area $2\pi r \cdot dr$ within the ring of (infinitesimal) extension dr at a radial location r.

Volume Definition and Loss

Liquid transfer through an LUO and its connected downstream valve may be associated with a volume U_{loss} left behind in the structure Γ after completion. Depending on the fluidic process of emptying of a CP-DF siphon valve, the lost amount of liquid

$$0 \leq U_{\text{loss}} \leq (A_0 + A) \cdot (R - R_{\text{crest}}) + U_{\text{iso}} \tag{17}$$

might vanish for a perfect "pulley" mechanism, which maintains a continuous liquid column until the entire liquid in Γ is dragged through the crest channel, and a in a pure "overspill" mode until $\Delta r = 0$ (Figure 1d). For serial processing, the volume arriving at the next valve $U_0' = U_0 - U_{\text{loss}}$ can be factored into its retention rate $\Omega' = \Omega(U_0')$, and into the mixing ratio of a quantitative bioassay. The metric

$$\overline{U_{\text{loss}}} = \frac{U_{\text{loss}}}{U_0} \tag{18}$$

is useful to quantify relative volume loss. For siphoning, where significant liquid volume may stay in Γ, $\overline{U_{\text{loss}}}$ may be minimized through U_{iso} and $A \cdot Z$. As any uncertainty ΔU_{loss} directly impacts the spread of the retention rate $\Delta\Omega' = \Delta\Omega(\Delta U_{\text{loss}})$, minimizing the relative fluctuation

$$\overline{\Delta U_{\text{loss}}} = \frac{\Delta U_{\text{loss}}}{U_{\text{loss}}} \tag{19}$$

is critical for assuring reliability towards fluidic LSI.

Reliability and Band Width

Preprints (www.preprints.org) | NOT PEER-REVIEWED | Posted: 22 April 2021 doi:10.20944/preprints202104.0612.v1

In practice, all experimental input parameters $\{\gamma_k\}$ impacting the liquid distribution $\Lambda = \Lambda(R, \Gamma, U_0, \omega)$, and thus Ω (11), are subject to random variation $\{\Delta\gamma_k\}$ delineated by a Gaussian distribution. This spread implies that at a given spin speed ω, the actual (radial) position of the meniscus $r'(\omega)$ will statistically vary around its target value $r(\omega)$. So, to make sure that the conditions for operationally reliable flow control are guaranteed, the spin rate ω has to stay outside the corridor $\Omega - M \cdot \Delta\Omega < \omega < \Omega + M \cdot \Delta\Omega$; in other words, ω has to be lifted or lowered through this entire frequency span for assuring proper retention and release for high- and low-pass valves, respectively.

The factor $M \in \{1,2,3,4\}$ represents the degree of (component-level) reliability, with probabilities $P_M = \mathrm{erf}\,[M/\sqrt{2}] \approx \{68\%, 95\%, 99.7\%, 99.99\%, \ldots\}$ (and "erf" representing the error function) that the actual values Ω' are found in this frequency interval. Above $M = 6$ and $M = 7$, reliability of this (single) valving step is in the range of 10 and 1 defects per million opportunities (DPMO); for $M = 8$, faults are practically absent.

At least in case that the input parameters $\{\gamma_k\}$ are (widely) independent and their spreads $\{\Delta\gamma_k\}$ comparatively small, Gaussian error propagation provides an analytical formula to calculate the standard deviation

$$\Delta\Omega \approx \sqrt{\sum_k \left(\frac{\partial\Omega}{\partial\gamma_k} \cdot \Delta\gamma_k\right)^2} \tag{20}$$

of Ω (11), which is very suitable method for optimization routines. Alternatively, Monte-Carlo (MC) methods can be interpreted as a virtual manufacture and testing by running (a large number of) N iterations, where a set of values $\{\gamma_k'\}$ is obtained from a random number generator assuming Gaussian distributions of $\{\gamma_k'\}$ of standard deviations $\{\Delta\gamma_k\}$ around their nominal values $\{\gamma_k\}$ and inserted into equation (11) for obtaining a histogram for Ω' in the simulated experiment.

These band widths $\Delta\Omega$ (20), which are associated with concurrently loaded valves, and thus change over the course of an LUO sequence, need to "fit" into the practically available envelope of spin rates ω between $\omega_{\min}$ and $\omega_{\max}$; these boundaries are, on the lower end at $\omega_{\min}$, constrained by a minimum centrifugal field f_ω (1) or pressure p_ω (2) required to stabilize a liquid distribution Λ, e.g., to suppress unwanted capillary motion (9); the upper value at $\omega_{\max}$ is imposed by factors such as the limited torque of the spindle motor τ_{spindle} (10), the pressure tightness of the (bonded) lid, and operational safety.

Towards multiplexing, the metric

$$\overline{\Delta\Omega} = \frac{\Delta\Omega}{\omega_{\max} - \omega_{\min}} \tag{21}$$

rewards minimum use of band width $\Delta\Omega$ (20) with respect to the available frequency envelope.

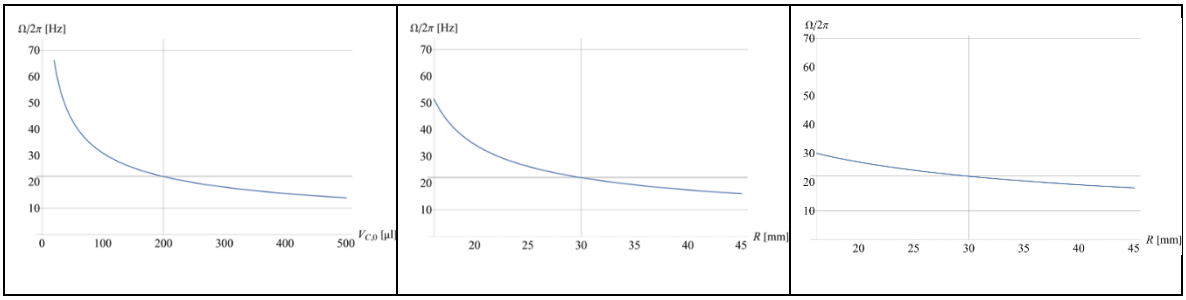

Preprints (www.preprints.org) | NOT PEER-REVIEWED | Posted: 22 April 2021 doi:10.20944/preprints202104.0612.v1

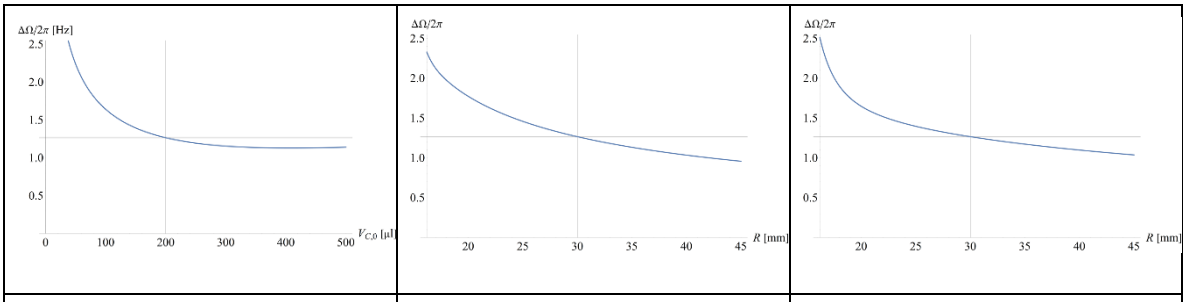

(a) Ω and $\Delta\Omega$ with volume of main compression chamber $V_{C,0}$.

(b) Ω and $\Delta\Omega$ with radial position R of Γ.

(c) Ω and $\Delta\Omega$ with position R of Γ for a field strength $f_\omega = \text{const.}$ (1).

Figure 2 Variation of retention rate Ω (11) and its spread $\Delta\Omega$ (20) with (a) the volume of the main, permanently gas filled compartment of the compression chamber $V_{C,0}$ and (b) the radial position R while leaving (the remainder of) the structure Γ unchanged. While Ω sharply increases towards shrinking compression volumes $V_{C,0}$ and central placements R, this comes at the expense of widening the tolerance $\Delta\Omega$. The gridlines represent the default volume $V_{C,0} = 200$ µl, radial position $R = 30$ mm and retention rate $\Omega/2\pi \approx 22$ Hz. (c) Ω and $\Delta\Omega$ vs R while maintaining the field strength f_ω (1) evaluated for its default geometry Γ (Appendix A) and its resulting critical rate $\Omega(R, \Gamma)$ at values $\varrho = 1000$ kg m^{-3}, $R = 3$ cm while varying the radial position R.

Multiplexing

System-Level Robustness

Towards microfluidic LSI, a multitude of such serial and parallelized valving steps needs to be coordinated on the LoaD device; each component failure might affect overall reliability. For N independently operating, concurrently loaded valves $\{i,j\}$ in a given step i, the probability for consistent system level function amounts to $(P_M)^N$; for the example of $M = 2$, and thus $P_M = 95\%$, $(P_{M=2})^N$ drops from approximately 90% to 86%, 77% and 60% for $N = \{2,3,5,10\}$, respectively, in case the bands $\Omega_{i,j} - M \cdot \Delta\Omega_{i,j} < \omega < \Omega_{i,j} + M \cdot \Delta\Omega_{i,j}$ must be avoided for properly controlling each valve i,j. For $N = 5$ active valves, extending the protected frequency intervals from $M = 2$ to $M = 3$ would significantly improve the (fluidic) reliability at system level from $(P_{M=2})^5 = 77\%$ to $(P_{M=3})^5 = 98.5\%$.

Note that the above considerations apply to each step i separately, i.e., after opening a particular valve $\{i,j\}$ at T_i, a new suite of loaded valves emerges; this fresh set consists of the valves that remained closed in i, plus the ones next in line to receive the released liquid, excluding end-point chambers. The protected areas in the frequency domain thus change over the course of the centrifugally multiplexed assay protocol $\omega(t)$.

Frequency Corridor

We consider valving steps $\{i\}$ with critical spin rates $\{\Omega_i\}$ that are activated at points in time $\{T_i\}$; each Ω_i represents a subset of concurrently loaded and opened valves $\{i,j\}$. Retention is assured while the spin rate $\omega(t)$ does neither surpass or drop below the (aggregate) band widths $2 \cdot M \cdot \max_j\{\Delta\Omega_{i,j}\}$ centered at the critical frequencies $\{\hat{\Omega}_i\}$ and $\{\check{\Omega}_i\}$ for $t < T_i$ for high- and low-pass valves, respectively. Figure 3a displays the scenario in frequency space for rotational actuation. An initial retention corridor between $\check{\Omega}_1$ and $\hat{\Omega}_2$ successively broadens as further valves are triggered, with $\hat{\Omega}_I < \hat{\Omega}_{i>I}$ and $\check{\Omega}_I > \check{\Omega}_{i>I}$.

Preprints (www.preprints.org) | NOT PEER-REVIEWED | Posted: 22 April 2021 doi:10.20944/preprints202104.0612.v1

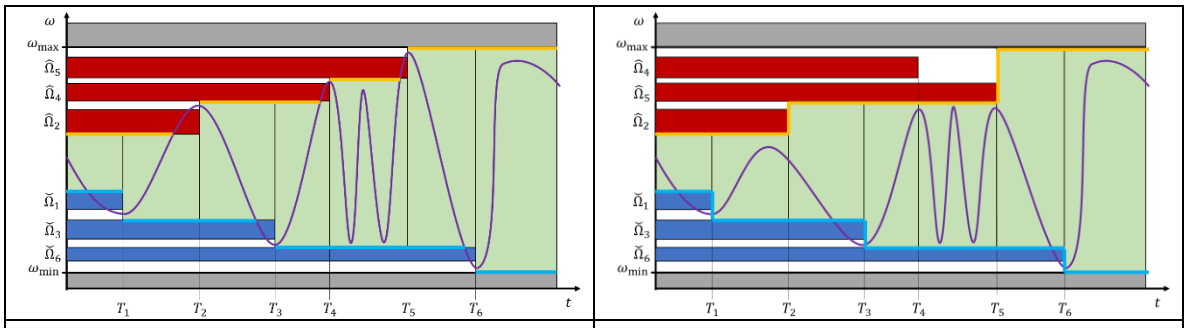

(a) Rotationally actuated valving. (b) Liquid release by venting.

Figure 3. Multiplexing of concurrently loaded valves in frequency vs time domain. High- and low-pass valving takes place at points in time $\{T_i\}$. With each step i, the frequency corridor (green) that is available for LUOs rearranges. (a) For rotational actuation, reliable opening of valves $\{I,j\}$ in a given step $i = I$ is triggered by crossing their linked frequency bands $\{\Omega_{I,j} \pm M \cdot \Delta\Omega_{I,j}\}$. (b) In venting mode, the concurrently loaded valves serially release according to the order of opening their compression chamber, i.e., $V_{\mathrm{C},0,i} \mapsto \infty$.

For the case of actuating (high-pass) CP valves by venting at $\{T_i\}$ with $i \in \{2,4,5\}$ in the exemplary scenario portrayed in Figure 3b, the retention zone for the spin rate curve $\omega(t)$ is also defined by the innermost limits of the allowed bands $\{\Omega_{i,j} \pm M \cdot \Delta\Omega_{i,j}\}$ of the valves still loaded at a given point in time T_i. Nevertheless, the order of release is merely imposed by the venting sequence, and does hence not necessitate a steadily rising or decreasing critical retention rates $\widehat{\Omega}_i$ and $\breve{\Omega}_i$ at T_i, respectively.

Configuration in Real and Frequency Space

Theoretically, the geometry Γ can always be modified to minimize the radial product $\bar{r}\Delta r$ (3), thus allowing any, randomly large retention rate $\Omega \propto 1/\sqrt{\bar{r}\Delta r}$ (11) for a given radial position R and liquid volume U_0. Yet, its statistical spread $\Delta\Omega$ (20) might become too big to still be able to sufficiently multiplex flow control within the confinement of the practical spin rate envelope between $\omega_{\min}$ and $\omega_{\max}$ (Figure 2 and Figure 3). Furthermore, there would be additional restrictions to parameter spaces, e.g., on the smallest feature sizes and tolerances $\{\Delta\gamma_i\}$ (20) linked to the manufacturing technology, or minimum liquid volumes, for instance, as prescribed by the loading and metering technique, the bioassay protocol, or the detection technology.

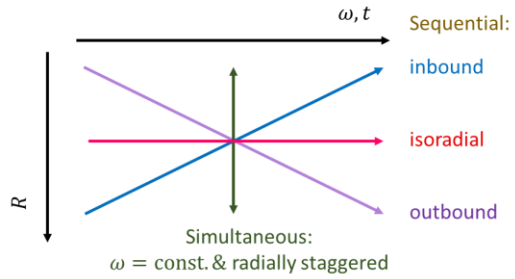

Figure 4. Representative scenarios underpinning multiplexing. The critical retention rates $\{\Omega_{i,j}\}$ (11) of concurrently loaded (high-pass) valves $\{i,j\}$ to be rotationally actuated at a time T_i may be preserved while shifting the radial positions $\{R_{i,j}\}$ of the structures $\{\Gamma_{i,j}\}$, e.g., to meet spatial requirements towards more crowded disc layouts, by adjusting the (permanently gas-filled part) of the compression chamber of volume $V_{\mathrm{C},0}$, while observing proper arrangement in the frequency domain ω, e.g., $\Omega_i + M \cdot \Delta\Omega_i < \Omega_{i+1} - M \cdot \Delta\Omega_{i+1}$.

It also needs to be considered that, especially towards concentrated packing of LoaD substrates, it is wise to leave the liquid carrying parts of geometries Γ, that may have already been thoroughly validated in terms of design-for-manufacture (DfM), fluidic and assay performance, untouched. For CP valving techniques, it is therefore advantageous to only alter larger, uncritical features, e.g., the

Preprints (www.preprints.org) | NOT PEER-REVIEWED | Posted: 22 April 2021 doi:10.20944/preprints202104.0612.v1

main volume $V_{C,0}$ of the permanently gas-filled part of the compression chamber (Figure 2a), for tuning Ω (11). Different U_0 may simply be accommodated by adjusting the width of the inlet reservoir. Nonetheless, the paucity of central disc space may necessitate shifting the radial location R, while the retention rate Ω (11) still needs to comply with the planned valving sequence (Figure 4).

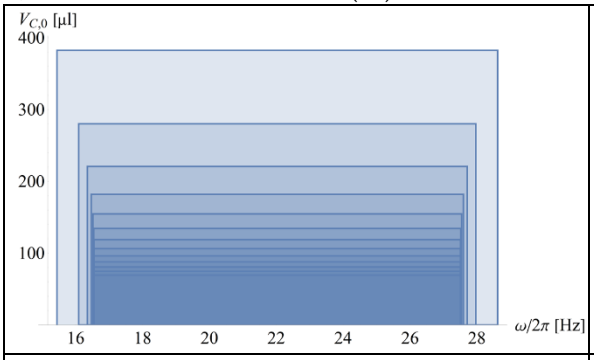

(a) Simultaneous opening of valves which are radially staggered at 1-cm intervals while releasing at the default spin rate $\Omega/2\pi \approx 22$ Hz. Both, moving to small R_i and large $V_{C,0,i}$, lead to a steep increase in $\Delta\Omega_i$ with respect to outer positions R.

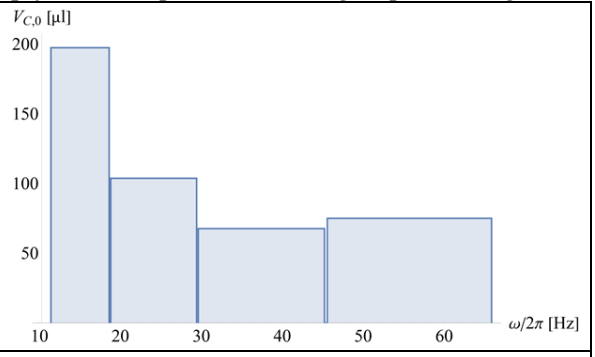

(b): Radially inbound release sequence with radial staggering at 1-cm intervals, starting with $\Omega_{i=1}/2\pi = 15$ Hz at $R_{i=1} = 5$ cm. Note that without factoring in tolerances, even $V_{C,0,i} = \text{const.}$ would assure proper sequential release while steadily raising ω.

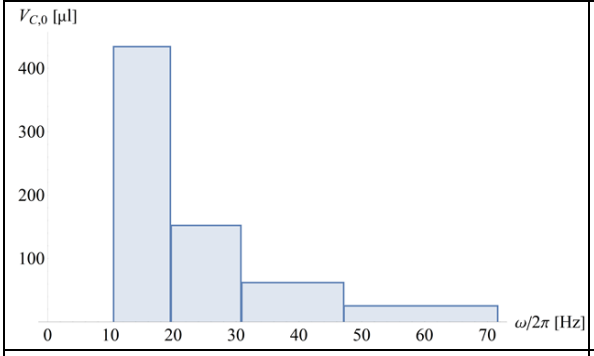

(c) Sequential release for isoradial placement at $R_i = 3$ cm. The largest $V_{C,0,i}$ with the smallest $\Delta\Omega_i$ is required for the first step $i = 1$.

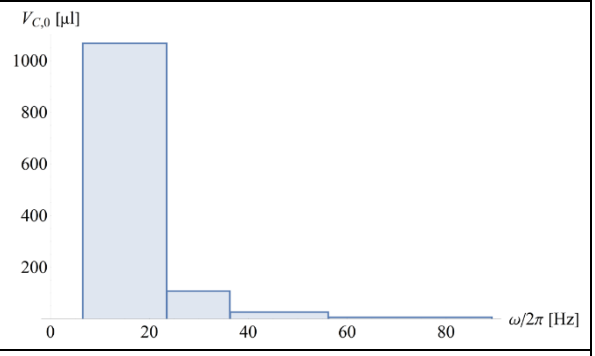

(d) Radially outbound sequential release at 1-cm intervals starting with $R_{i=1} = 2$ cm. Note that the critical spin rate $\Omega > \omega_{\max}$ of the final valve falls outside the practically available ω-envelope.

Figure 5. Distribution of bands in frequency space ω with required volumes of the main compression chamber $V_{C,0,i}$ for the different radial staggering and release scenarios portrayed in Figure 4. CP-DF siphon valves $\{i,j\}$ to be released simultaneously, i.e., $T_i = T_{i+1}$, or sequentially, i.e., $T_i < T_{i+1}$; the valves, which have similar geometries $\Gamma_{i,j}$ of their liquid-occupied sectors and downstream compression volumes $V_{C,0,i,j}$, are placed isoradially, i.e., $R = 3$ cm, or staggered over radial positions $R = \{2,3,4,5\}$ cm. The reliability factor is $M = 4$. (a) A set of radially staggered valves $\{i,j\}$ with $R_{i,j} > R_{i,j-1}$ has been tuned through their $V_{C,0,i,j}$ to simultaneously burst in the same step i once $\omega > \Omega_i + M \cdot \Delta\Omega_i$ with $\Delta\Omega_i = \max\{\Delta\Omega_{i,j}\}$. There are three representative cases for sequential actuation with $\Omega_i - M \cdot \Delta\Omega_i > \Omega_{i-1} + M \cdot \Delta\Omega_{i-1}$ for successive steps i according to $\Omega_i > \Omega_{i-1}$. (b) For identical $\Gamma_{i,j}$ and $V_{C,i,j}$, the valves will open according to their radially inbound order $R_i < R_{i-1}$. (c) For isoradial alignment $R_i = R = \text{const.}$, the valve with the largest V_C opens first: $V_{C,i} < V_{C,i-1}$. (d) Also, a radially outbound opening sequence $R_i > R_{i-1}$ can be achieved for which $V_{C,i}$ needs to be drastically reduced along successive steps i to suppress premature release from by the high pressure p_ω at distal locations, which comes at the expense of huge bandwidth $\Delta\Omega$.

Figure 4 shows distinctive scenarios for CP-DF siphon valves commonly encountered when seeking the best compromise in real and frequency space. We again consider simultaneous actuation

Preprints (www.preprints.org) | NOT PEER-REVIEWED | Posted: 22 April 2021 doi:10.20944/preprints202104.0612.v1

of valves $\{i,j\}$ at times $\{T_i\}$, and sequential firing with isoradial as well as radially inbound and outbound staggering on the given disc. The ordering of Ω_i (11) is accomplished by adjusting $V_{C,0}$, while leaving all other parts of Γ and U_0 unchanged. Note, again, that without non-rotationally powered pumping mechanisms, a given liquid distribution Λ_i can only migrate radially outbound, i.e., $R_{i+1} > R_i$.

Figure 5 displays the distribution of the frequency bands $\{\Omega_i \pm M \cdot \Delta\Omega_i\}$ in the different rotational actuation scenarios for simultaneous and sequential release (Figure 4) through adjusting the main volume of the compression chamber $V_{C,0,i,j}$. Note that the requirement to create non-overlapping bands $\Omega \pm M \cdot \Delta\Omega$ for serial opening even leads to a slight increase in $V_{C,0}$ towards the highest spin rate ω (Figure 5b), and a huge widening of frequency bands $\Omega \pm M \cdot \Delta\Omega$ in the radially outbound release sequence (Figure 5d).

Exemplary Bioassay Panel

Figure 6 illustrates the rotational automation of a typical bioassay protocol. Plasma P I separated from a (blood) sample S before mixing with a first, onboard stored liquid reagent L1. This mixture P&L1 is then released to a final detection chamber, where it is successively mixed with reagents L2 and L3. The liquid handling is coordinated by high-pass valves opening after their respective bands $\Omega_i \pm M \cdot \Delta\Omega_i$ are crossed, thus creating an ω-corridor with a successively growing upper limit over time t. Intermediate mixing steps are implemented by zig-zig patterns in $\omega(t)$. The domains available in real and frequency space are confined by R_{min} and R_{max}, and ω_{min} and ω_{max}, respectively.

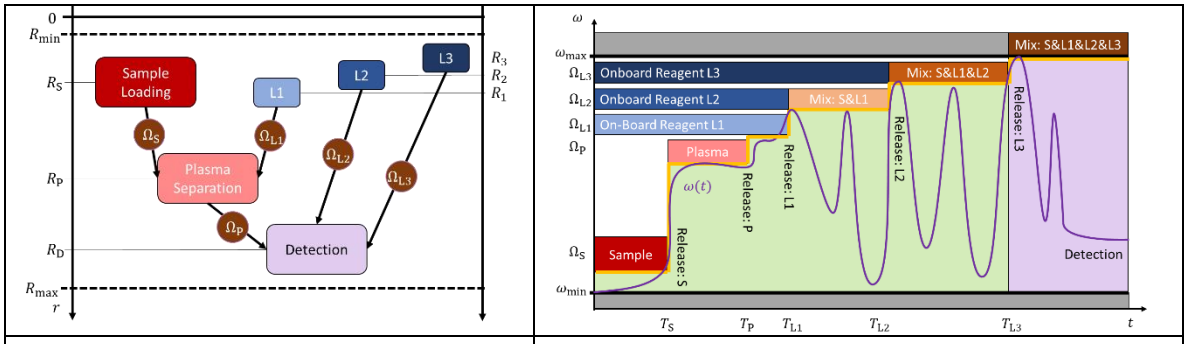

(a) Spatial arrangement and connections. (b) Spin protocol $\omega(t)$.

Figure 6 Exemplary bioassay with loading of blood sample, plasma separation, mixing with prestored liquid reagents L_i. Flow is controlled by five high-pass valves with release rates $\omega_{min} < \Omega_i < \omega_{max}$ located at $R_{min} < R_i < R_{max}$ and opening for $\omega > \Omega_i$ at points in time T_i. (a) Plasma separation takes place in a peripheral position R_P at high field strength $f_\omega \propto R_P \cdot \omega^2$ (1). While, owing to the unidirectional nature of the centrifugal field, the course of the assay requires $R_S < R_P < R_D$ and $R_{L1} < R_P$, a radially inbound staggering $R_{L1} > R_{L2} > R_{L3}$ (Figure 5b) has been chosen for the serial release of $\{L_i\}$ through their high-pass valves opening at $\Omega_{L1} < \Omega_{L2} < \Omega_{L3}$. (b) A blood sample S is loaded and released at $\Omega_S < \omega < \Omega_P$. Separation of plasma P proceeds at $\Omega_P < \omega < \Omega_{L1}$. Onboard liquid reagent L1 is then forwarded at $\Omega_{L1} < \omega < \Omega_{L2}$ into the separation chamber where it is mixed with the plasma P within $\omega_{min} < \omega < \Omega_{L2}$. The mixture P&L1 is then forwarded to the final detection chamber for $\Omega_P < \omega < \Omega_{L2}$, followed by addition of and mixing with L2 within $\Omega_2 < \omega < \Omega_3$ and $\omega_{min} < \omega < \Omega_{L3}$, respectively. Finally, L3 is added at $\Omega_3 < \omega < \omega_{max}$ and mixed S&L1&L2 within $\omega_{min} < \omega < \omega_{max}$. The green background marks the allowed frequency corridor at each point in time $t = T_i$, with its upper limit expanding according to $\omega_{min} < \Omega_S < \Omega_P < \Omega_{L1} < \Omega_{L2} < \Omega_{L3} < \omega_{max}$. Note that, for the sake of simplicity, the frequency thresholds $\{\Omega_i\}$ are meant to refer to their associated bands $\Omega_i \pm M \cdot \Delta\Omega_i$.

The unidirectional nature of the centrifugal field f_ω (1) requires that the positions of the serial processing of the sample through loading, separation and detection chambers needs to follow $R_S <$

Preprints (www.preprints.org) | NOT PEER-REVIEWED | Posted: 22 April 2021 doi:10.20944/preprints202104.0612.v1

$R_P < R_D$, while the release rates of the high-pass valves need to continuously increase along $\omega_{min} < \Omega_S < \Omega_P < \Omega_{L1} < \Omega_{L2} < \Omega_{L3} < \omega_{max}$, so that their associated bands $\Omega_i \pm M \cdot \Delta\Omega_i$ do not overlap. In the portrayed exemplary assay protocol, high-quality and speedy plasma separation is linked to a large field strength $f_\omega \propto R_P \cdot \omega^2$ (1) which is limited by the $\omega < \Omega_P$ (11), thus making an outer position R_P favorable. On the other hand, high retention rates $\Omega_P < \Omega_{L,i} \propto 1/\sqrt{\bar{r}_i \Delta r_i}$ (11) for the onboard reagents within the narrow corridor $\Omega_P < \omega < \omega_{max}$ are best achieved for their more central placement (when estimating $\bar{r}_i \approx R_{L,i}$ and $\Delta r_i \approx$ const.).

Overall, the structures $\{\Gamma_{i,j}\}$ presenting LUOs with their downstream valves need to meet several, partially contradictory demands on the maximum retention rate Ω (11), disc real estate $\bar{A}$ (16), maximum field strength $\hat{f}_\omega$ (12), and footprints in radial $\bar{R}$ (14), $\overline{\Delta R}$ (15) and frequency space $\overline{\Delta\Omega}$ (21).

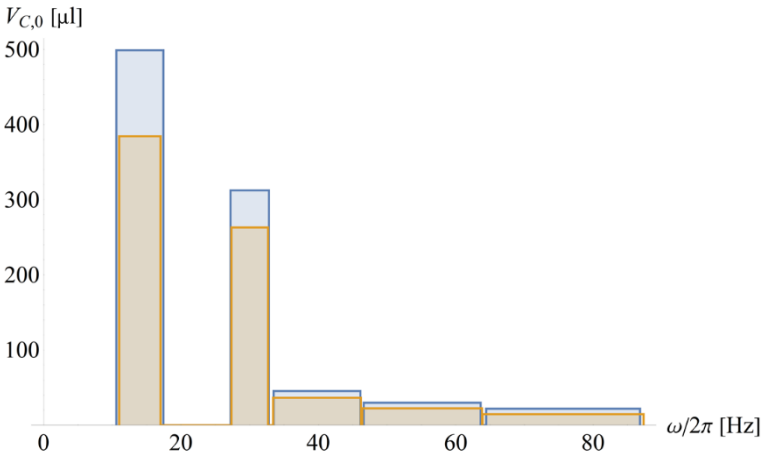

Figure 7 Rotational automation of exemplary bioassay and sequential release of sample and plasmas well as pre-stored liquid onboard reagents L1, L2 and L3 with high-pass CP-DF siphon valves of release rates $\{\Omega_i\}$ with $\Omega_S/2\pi = 15$ Hz and $\Omega_P/2\pi = 30$ Hz. The release rates are tuned by the dead volume of the main compression chamber $\{V_{C,0,i}\}$ as displayed on the vertical axis. (a) Radial positions (blue) R_i={3,4,3.5,3,2.5} cm and (orange) $R_i' = R_i + 0.5$ cm mimicking concurrent processing of identical bioassay protocols requiring identical $\{\Omega_i\}$ for concurrent valving ($M = 3$) while increasing their spatial packing density towards microfluidic LSI.

Figure 7 shows the release rates $\{\Omega_i\}$ for given $\Omega_S/2\pi = 15$ Hz and $\Omega_P/2\pi = 30$ Hz (at $R_P = 4$ cm) of CP-DF siphon valves with the same default geometries Γ_i, except for their (main) compression volumes $\Gamma_{C,0,i}$ which are varied to guarantee disjunct tolerance intervals $\{\Delta\Omega_i\}$ for a given $M = 3$. The two distributions represent sets of identical $\{\Omega_i\}$ with their radial positions $\{R_i\}$ shifted by 0.5 cm as a possible method to increase the functional integration density on a given disc space, e.g., to concurrently measure different biosamples, calibrants, dilution series or redundancies for statistics. Note that the rotational actuation of these high-pass valves "squeezes" the release rates for the onboard reagents $\{\Omega_{L,i}\}$ in the narrow ω −strip within $\Omega_P + M \cdot \Delta\Omega_P < \omega < \omega_{max}$ (see also Figure 6b).

Assay Parallelization

A straight-forward method to replicate several simultaneously processed, identical assay protocols on the same LoaD carrier, e.g., for testing different samples for the same analytes, or for redundancies for controls, calibration, or statistics, is to equalize their release frequencies $\{\Omega_i\}$ which are crossed synchronously $\{T_i\}$. The packing density might be increased by radial staggering of the structures Γ, for which Figure 2 teaches the required adjustments of the main compression volumes $V_{C,0,i,j}$ and the impact of the total band width $2 \cdot M \cdot \Delta\Omega_i$. Concurrent processing of homologous assay protocols with deviations of inlet volumes $U_{0,i}$ may be readily compensated by adjusting the width

Preprints (www.preprints.org) | NOT PEER-REVIEWED | Posted: 22 April 2021 doi:10.20944/preprints202104.0612.v1

of the inlet reservoirs. In the general case of multiplexing diverging protocols, each release step must comply with the frequency corridor required to reliably retain concurrently loaded valves.

Advanced Rotational Flow Control

This section expands on the actuation mode of CP-DF siphon valves by venting (Figure 1d). Instead of the various mechanical, radiation-induced, or thermal methods to open the compression chamber, a second (ancillary) liquid volume wets a DF placed at a remote location to effectuate $p_V \mapsto p_0$. First, a hand-shake mechanism called event-triggering is introduced, which also enable logical flow control. Afterwards, the timing of event-triggering, e.g., to comply with mixing or incubation periods of bioassays, through delay elements and rotational pulsing are elaborated.

Event-Triggering

We now attach two DFs to the compression chamber of CP-DF siphon valves (Figure 8). In an exemplary assembly of upper and lower layers displaying the microfluidic conduits sandwiching a sealing sheet containing a set of DFs, the first "Load Film" (LF) initially blocks the outlet for the liquid through a vertical via into a lower layer; a second "Control Film" (CF) is placed in a pneumatically connected, distal compartment [48]. Below a critical spin rate Ω (11), the pneumatic counterpressure p_V (8) prevents the liquid from reaching the LF.

The remote CF can be accessed by another, ancillary liquid through a channel in the lower layer to open the DF, and to thus massively expand the enclosed gas volume $V_C \mapsto \infty$. With $p_V \mapsto p_0$, the main liquid advances into the chamber containing the LF, which then disintegrates for release through the exit channel.

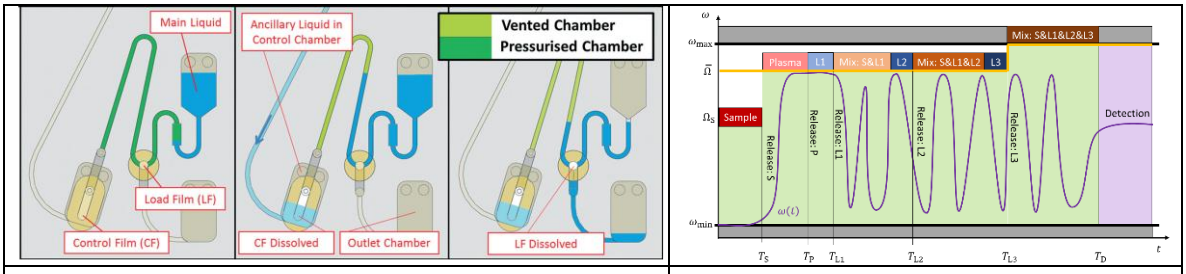

(a) Basic configuration. (b) Spin protocol $\omega(t)$.

Figure 8. Principle of event-triggered flow control. (a) Basic valve configuration with the control film (CF) which is opened by a first liquid to vent the compression chamber of a pneumatic valve, thus releasing a second liquid through the load film (LF) (adopted from [48]). (b) Extended corridor for the spin rate $\omega(t)$ in case of the event-triggered vs the rotationally actuated (Figure 6a) high-pass valves. After the sample is released at $\omega > \Omega_S$, the upper boundary is given by the, e.g., common, retention rate $\overline{\Omega}$ shared by all LUOs. Release from their chambers is prompted by event-triggered venting, rather than raising the spin rate ω.

Event-triggering (Figure 8) refers to the constellation when a liquid received from a preceding stage of an assay protocol takes on the role of the ancillary liquid to establish a "hand-shake" type flow control; instead of rotational cues or external power, sequential release follows a "domino effect" that proceeds widely independent of the spin rate $\omega(t)$. The frequency corridor (Figure 3), and especially the maximum field strength $\hat{f}_\omega$ (12) that is available for LUOs along the assay procedure, are thus only restricted by the (minimum) retention rate Ω (11) of concurrently loaded (high-pass) valves, or $\omega_{\max}$.

Preprints (www.preprints.org) | NOT PEER-REVIEWED | Posted: 22 April 2021 doi:10.20944/preprints202104.0612.v1

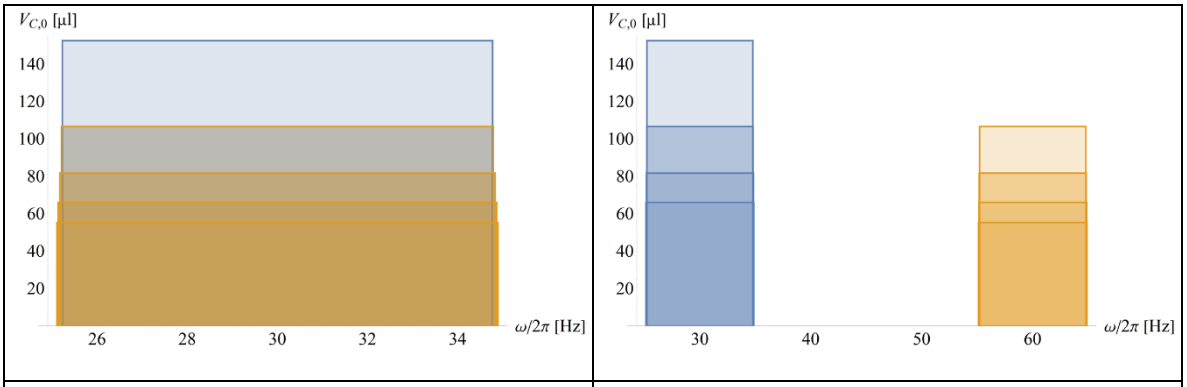

(a) Default (blue) and radially shifted (orange) alignment of valves $\{\Gamma_i\}$.

(b) Separation frequencies $\Omega_P = 30$ Hz (blue) and 60 Hz (orange).

Figure 9 Event-triggered flow control in exemplary bioassay protocol. (a) The set of valves $\{\Gamma_i\}$ in at their default (blue) position $\{R_i\}$ and radially shifted outwards by 0.5 cm (orange) which is a common requirement towards microfluidic LSI. All frequency bands $\{\Omega_i \pm M \cdot \Delta\Omega_i\}$ are centered at the same rate $\Omega_i = \Omega$. (b) The same radial distribution $\{R_i\}$ is operated at different spin rates $\Omega_i = \Omega_P$, showing that event-triggering is favorable for enabling high spin rates ω, e.g., for plasma separation.

Figure 9 illustrates the benefits of event-triggered flow control regarding the configurability as well as packing density in real and frequency space. As opposed to the implementation of the exemplary bioassays with the rotationally actuated high-pass CP-DF siphon valves (Figure 7), the liquid reagents $\{L_i\}$ may be released at the same rate $\omega > \Omega_P + M \cdot \Delta\Omega_P$ as the plasma separation at Ω_P. Overall, the speed (and quality) of plasma separation in the initial stages of common assay protocols may hence be significantly improved.

Logical Flow Control

Such an event-triggered relay may also be considered as a logical "IF" condition, in a way that a (subsequent) valve only fires "if" another liquid has arrived to dissolve the CF in a designated pneumatic compartment [48]. This concept has been further refined by placing the CF at critical radial positions R_{DF} (Figure 1a) in a way that a minimum liquid volume U_{CF} must arrive in the DF chamber to dissolve the membrane, and thus vent and open the next valve. Based on such a logical "IF" condition, closed-loop "handshake" flow control has been implemented. Alternatively, the DF in the receiving chamber may be placed at a radial position which is only reached after a minimum amount of liquid has entered from a set of incoming channels, thus establishing an "AND" element. In a similar way, an "OR" condition may be defined by positioning the DF so that it is wetted after the arrival of a minimum liquid volume from a defined subset of incoming channels.

Delay Elements

Bioassay protocols usually require certain time spans, e.g., to account for reaction kinetics between bioentities that are dissolved, suspended, or bound to surfaces on cells, beads of walls. However, event-triggering "hard-wires" intervals in the network of valving structures in a direct "knock-on" fashion. To this end, delay elements have been incorporated into event-triggered fluidic systems for bioassay integration [61]. Examples are hydrodynamic flow resistances imposed by narrow and long channel segments or paper strips, which have also been utilized for other purposes [11, 62]. Through imbibition or wicking, these timers slow down the transfer of the main or ancillary liquid compared to open channels. While, in theory, also reducing the spin speed during transfer periods would be an option, such action would require rather complex "closed-loop" coordination between monitoring liquid flow on the disc and the speed of the spindle motor ω.

Pulsing of Spin Rate

Preprints (www.preprints.org) | NOT PEER-REVIEWED | Posted: 22 April 2021 doi:10.20944/preprints202104.0612.v1

Commonly, the aggregate time spans for dissolution and liquid transfer range on the second- to minute scale, while bioassays often require processing times of minutes to hours. So, while such physical delay elements prolong the intervals available for LUOs, the timing still faces upper limits, and it is also 'inscribed' in the layout and material characteristics, such as the dissolution time of the sacrificial membrane or the imbibition speed of the paper strip. In addition, the requirement of the rotational actuation mode to steadily increase the critical spin rates Ω_i along successive steps i managed by high-pass CP valves compromises the flexibility that may be required for enabling microfluidic LSI.

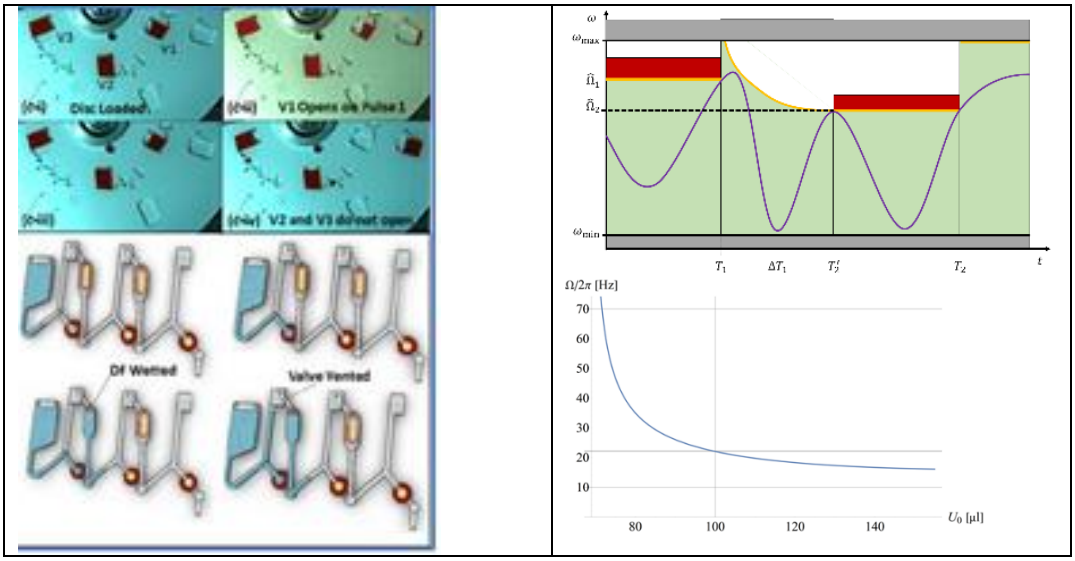

Figure 10. Pulse-actuated CP-DF valving (adopted from [49]). (a) Photo and concept of structure. (b) Spin protocol $\omega(t)$ and decrease of the retention frequency Ω with the arrival of the liquid volume U_0. In conventional CP-DF valving (a), a set of liquids are released sequentially through stepping up the spin rate ω to their critical burst frequencies $\{\Omega_i\}$. Digital pulse actuation considers the time it takes a liquid volume to advance through the outlet channel between valve opening at the burst frequency Ω_i and its arrival at the following valve characterized by Ω_{i+1}. During this interval ΔT, which is primarily determined by the centrifugally induced pressure head p_ω (2), the flow resistance of the connecting channel and the dissolution time of the DF, the spin rate ω is decreased below Ω_{i+1}, including the option $\Omega_{i+1} < \Omega_i$, which is not possible in the original arrangement. (c) Evolution of the critical spin rate $\Omega(t)$ with the arrival of liquid volume $U_0(t)$ in serial valving. During loading of the next valve $i+1$ within the interval ΔT_i, its retention rate $\Omega_{i+1}(t)$ always resides above the nominal rate $\Omega(U_0)$ after the entire volume U_0 has arrived, e.g., $\Omega/2\pi \approx 22$ Hz for $U_0 = 100$ µl as indicated by the horizontal gridline.

For situations when liquid volumes $\{U_{i,j}\}$ are transferred in parallel between steps $\{i\}$ at $\{T_i\}$, each involving a set of $\{i,j\}$ loaded valves, the concept of rotational pulsing (Figure 10) has been presented [49]. This flow control mechanism exploits that within the interval $\Delta T_i = T_{i+1} - T_i$, the spin rate $\omega(T_i < t < T_{i+1})$ only needs to stay inside the corridor required to retain the (other) concurrently loaded liquids; furthermore, during the following interval ΔT_i, the spin rate ω may be reduced below Ω_i, thus alleviating the requirement for steady increase (Figure 7) or maintaining constant spin rate ω (Figure 8 and Figure 9) while sequentially progressing the release steps $\{i\}$. Note that during the filling of the subsequent valve, retention rate converges from the upper side towards Ω (11), thus allowing higher spin rates ω than for LUOs than in its fully loaded state (Figure 10c).

Preprints (www.preprints.org) | NOT PEER-REVIEWED | Posted: 22 April 2021 doi:10.20944/preprints202104.0612.v1

In a similar way as 'venting', rotational pulsing allows to retain liquid menisci at sufficiently "safe" spacing from the DF during retention. It can also be used to synchronize parallel processes, e.g., when the same protocol needs to be run on several patient samples. However, in heterogeneous assay panels where each channel would run a different protocol, the height of the rotational pulse for the CP-DF valve i to be released is confined by the lowest critical frequency of the concurrently loaded valves k that need to stay closed, i.e., $\omega_{\mathrm{pulse},i} < \min_{k \neq i} \Omega_k - M \cdot \Delta M_k$.

Conclusions and Outlook

As key enablers in manifold life-science applications, sample-to-answer automation and parallelization of bioassays roots in fluidic large(r)-scale integration (LSI) at dense packing on the limited disc real estate. Within finite frequency corridors, sufficient system-level reliability, and high-performance, rotational processing of Laboratory Unit Operations (LUOs) pertaining to the bioanalytical assay protocols need to be facilitated.

To this end, this work has focused on modelling the centrifugal microfluidic working principles of rotationally controlled valving on "Lab-on-a-Disc" (LoaD) systems that are promising candidates for enabling cost-efficient and robust commercial solutions for decentralized testing, especially in low-resource settings and minimally trained operators. Among the various flow control schemes [37], so-called centrifugo-pneumatic (CP) dissolvable-film (DF) siphon valves have been further investigated due to their (potential for) low band width $\Delta\Omega$ (20), their high configurability, e.g., reflected by compensation of shifts of their radial position R by their compression volume V_C for maintaining the retention rate Ω (11), and their excellent amenability to advanced flow control, such as handshake-mode event-triggering, logical elements and digital pulsing.

Future work will extend the underlying digital twin modelling to include hybrid designs featuring different types of high- and low-pass valves, on-board storage of liquid and dry reagents, fluid dynamic effects and refined geometries, e.g., by including rounded edges and contours, multi-disc stacks and draft angles that are required for demolding in commercially common polymer replication techniques. Also externally powered, on-board pumping and control modules may readily be included [43, 63]. Furthermore, the design tool may be extended to include simulation of bioassay kinetics and manufacturing processes, e.g., mold flow analysis.

With its high predictive power, the presented work can thus enable automated generation and validation of designs regarding fluidic functionality and compliance with design-for-manufacture (DfM) guidelines, and related scale-up towards mass fabrication. Such software might then create an effective interface for foundry services as a hallmark of mature industrial supply chains in a task-sharing economy.

In view of the vanguard of strong, often disruptive socio-economic and technological trends in its technological environment, such as Maker / Fab Labs, hackathons, science as a service (SaaS), cloud computing, Machine Learning (ML) / Artificial Intelligence (AI), Big Data, Internet of Things (IoT) and decentralization, as well as the continuing expiry of all foundational patents on centrifugal microfluidics that were primarily filed throughout the 1990s and early 2000s, which creates sufficient wiggle room in intellectual property (IP) space, open platform models for heralding a new era of blockchain-backed participatory research models and crowdsourcing of ideas, expertise, skills, work force, infrastructure and equipment may be established [64-67].

Funding: This research received no external funding.

Conflicts of Interest: The author declares no conflict of interest.

Appendix A – Default Geometry of CP-DF Siphon Valves

Preprints (www.preprints.org) | NOT PEER-REVIEWED | Posted: 22 April 2021 doi:10.20944/preprints202104.0612.v1

The structure Γ, loaded liquid volumes U_0 and radial positions R can be varied across a multi-dimensional parameter space, e.g., to tune retention rates Ω of other key performance indicators. *Table S1* gives of overview or generic values which can be used to initiate optimization.

$R = 3$ cm	$R_{\min} = 1.5$ cm	$R_{\max} = 5.5$ cm	$R_{\mathrm{DF}} = 3.15$ cm $> R$
$A_0 = d_0 \cdot w_0$	$d_0 = 1$ mm	$w_0 = 5$ mm	
$U_0 = 100$ µl $< \mathrm{A}_0 \cdot (R - R_{\min})$			
$U_{\mathrm{iso}} = d_0 \cdot h \cdot L \ll U_0$	$d_{\mathrm{iso}} = 1$ mm	$h_{\mathrm{iso}} = 1$ mm	$L_{\mathrm{iso}} = 15$ mm $> w_0 + w$
$U_Z = d \cdot w \cdot Z$	$d = 500$ µm	$w = 800$ µm $\ll w_0$	$Z = 10$ mm
$V_{\mathrm{C},0} = d_{\mathrm{C}} \cdot w_{\mathrm{C}} \cdot h_{\mathrm{C}} \gg U_Z$	$d_{\mathrm{C}} = 1$ mm	$w_{\mathrm{C}} = 20$ mm	$h_{\mathrm{C}} = 10$ mm
$V_{\mathrm{int}} = d_{\mathrm{int}} \cdot h_{\mathrm{int}} \cdot L_{\mathrm{int}} \ll V_{\mathrm{C}}$	$d_{\mathrm{int}} = 200$ µm	$h_{\mathrm{int}} = 300$ µm	$L_{\mathrm{int}} = 1$ cm $> 2w$
$V_{\mathrm{DF}} = 0.25\pi \cdot d_{\mathrm{DF}} \cdot D_{\mathrm{DF}}^2 \ll V_{\mathrm{C}}$	$d_{\mathrm{DF}} = 190$ µm	$D_{\mathrm{DF}} = 3$ mm	$\alpha = 0.45, \beta = 0.5$

Table S1 Default geometrical parameters and relationships of CP-DF siphon valves (Figure 1). The resulting critical spin rate $\Omega(R, \Gamma, U_0)/2\pi \approx 22$ Hz. Minimum lateral dimensions are given by the smallest practical diameter of milling tools (200 µm). As tools for injection molding are often adopted from optical data storage (e.g., CD, DVD, Blu-ray), a central, 1.5-cm diameter hole and a disc radius of 6 cm with thickness around 1.2 mm, fluidic structures Γ may need to stay within the radial interval between $R_{\min} = 1.5$ cm and $R_{\max} = 5.5$ cm, and an upper limit for the depth of about 1 mm. The lowest depth of cavities is often restricted by the sealing technology; for large lateral extensions or small aspect ratios, sagging of the lid, which is often a foil, may significantly change the nominal volume capacity, also in response to the pressure, and might even lead to sticking to the bottom of the cavity.

References

1. Manz, A., N. Graber, and H.M. Widmer *Miniaturized total chemical analysis systems: A novel concept for chemical sensing*. Sensors and Actuators B: Chemical, 1990. **1**, 244-248 DOI: 10.1016/0925-4005(90)80209-I.
2. Madou, M.J. and G.J. Kellogg *The LabCD (TM): A centrifuge-based microfluidic platform for diagnostics*. Systems and Technologies for Clinical Diagnostics and Drug Discovery, Proceedings Of, 1998. **3259**, 80-93 DOI: 10.1117/12.307314.
3. Ducrée, J., S. Haeberle, S. Lutz, S. Pausch, F.v. Stetten, and R. Zengerle *The centrifugal microfluidic Bio-Disk platform*. Journal of Micromechanics and Microengineering, 2007. **17**, S103-S115 DOI: 10.1088/0960-1317/17/7/s07.
4. Gorkin, R., J. Park, J. Siegrist, M. Amasia, B.S. Lee, J.M. Park, J. Kim, H. Kim, M. Madou, and Y.K. Cho *Centrifugal microfluidics for biomedical applications*. Lab on a Chip, 2010. **10**, 1758-1773 DOI: 10.1039/b924109d.
5. Park, J.M., Y.K. Cho, B.S. Lee, J.G. Lee, and C. Ko *Multifunctional microvalves control by optical illumination on nanoheaters and its application in centrifugal microfluidic devices*. Lab on a Chip, 2007. **7**, 557-64 DOI: 10.1039/b616112j.
6. Watts, A.S., A.A. Urbas, E. Moschou, V.G. Gavalas, J.V. Zoval, M. Madou, and L.G. Bachas *Centrifugal microfluidics with integrated sensing microdome optodes for multiion detection*. Analytical Chemistry, 2007. **79**, 8046-8054 DOI: 10.1021/ac0709100.
7. Clime, L., D. Brassard, M. Geissler, and T. Veres *Active pneumatic control of centrifugal microfluidic flows for lab-on-a-chip applications*. Lab on a Chip, 2015. **15**, 2400-2411 DOI: 10.1039/c4lc01490a.

8. Strohmeier, O., M. Keller, F. Schwemmer, S. Zehnle, D. Mark, F. von Stetten, R. Zengerle, and N. Paust *Centrifugal microfluidic platforms: advanced unit operations and applications*. Chemical Society Reviews, 2015. **44**, 6187-229 DOI: 10.1039/c4cs00371c.
9. Thompson, B.L., C. Birch, D.A. Nelson, J. Li, J.A. DuVall, D. Le Roux, A.C. Tsuei, D.L. Mills, B.E. Root, and J.P. Landers *A centrifugal microfluidic device with integrated gold leaf electrodes for the electrophoretic separation of DNA*. Lab on a Chip, 2016. **16**, 4569-4580 DOI: 10.1039/c6lc00953k.
10. Smith, S., D. Mager, A. Perebikovsky, E. Shamloo, D. Kinahan, R. Mishra, S.M. Torres Delgado, H. Kido, S. Saha, J. Ducrée, M. Madou, K. Land, and J.G. Korvink *CD-Based Microfluidics for Primary Care in Extreme Point-of-Care Settings*. Micromachines (Basel), 2016. **7**, DOI: 10.3390/mi7020022.
11. Hwang, H., S.-H. Kim, T.-H. Kim, J.-K. Park, and Y.-K. Cho *Paper on a disc: balancing the capillary-driven flow with a centrifugal force*. Lab on a Chip, 2011. **11**, 3404 DOI: 10.1039/c1lc20445a.
12. Kim, T.H., H. Hwang, R. Gorkin, M. Madou, and Y.K. Cho *Geometry effects on blood separation rate on a rotating disc*. Sensors and Actuators B-Chemical, 2013. **178**, 648-655 DOI: 10.1016/j.snb.2013.01.011.
13. Hwang, H., H.H. Kim, and Y.K. Cho *Elastomeric membrane valves in a disc*. Lab on a Chip, 2011. **11**, 1434-6 DOI: 10.1039/c0lc00658k.
14. Roy, E., G. Stewart, M. Mounier, L. Malic, R. Peytavi, L. Clime, M. Madou, M. Bossinot, M.G. Bergeron, and T. Veres *From cellular lysis to microarray detection, an integrated thermoplastic elastomer (TPE) point of care Lab on a Disc*. Lab on a Chip, 2015. **15**, 406-416 DOI: 10.1039/c4lc00947a.
15. Kong, L.X., A. Perebikovsky, J. Moebius, L. Kulinsky, and M. Madou *Lab-on-a-CD*. Journal of Laboratory Automation, 2016. **21**, 323-355 DOI: 10.1177/2211068215588456.
16. Hess, J.F., S. Zehnle, P. Juelg, T. Hutzenlaub, R. Zengerle, and N. Paust *Review on pneumatic operations in centrifugal microfluidics*. Lab on a Chip, 2019. **19**, 3745-3770 DOI: 10.1039/C9LC00441F.
17. Aeinehvand, M.M., P. Magaña, M.S. Aeinehvand, O. Aguilar, M.J. Madou, and S.O. Martinez-Chapa *Ultra-rapid and low-cost fabrication of centrifugal microfluidic platforms with active mechanical valves*. RSC Advances, 2017. **7**, 55400-55407 DOI: 10.1039/c7ra11532f.
18. Aeinehvand, M.M., L. Weber, M. Jiménez, A. Palermo, M. Bauer, F.F. Loeffler, F. Ibrahim, F. Breitling, J. Korvink, M. Madou, D. Mager, and S.O. Martínez-Chapa *Elastic reversible valves on centrifugal microfluidic platforms*. Lab on a Chip, 2019. **19**, 1090-1100 DOI: 10.1039/C8LC00849C.
19. Nguyen, H.V., V.D. Nguyen, H.Q. Nguyen, T.H.T. Chau, E.Y. Lee, and T.S. Seo *Nucleic acid diagnostics on the total integrated lab-on-a-disc for point-of-care testing*. Biosensors and Bioelectronics, 2019. **141**, 111466 DOI: 10.1016/j.bios.2019.111466.
20. Rombach, M., S. Hin, M. Specht, B. Johannsen, J. Lüddecke, N. Paust, R. Zengerle, L. Roux, T. Sutcliffe, J.R. Peham, C. Herz, M. Panning, O. Donoso Mantke, and K. Mitsakakis, *RespiDisk: a point-of-care platform for fully automated detection of respiratory tract infection pathogens in clinical samples.* The Analyst, 2020. **145**(21): p. 7040-7047.
21. Miyazaki, C.M., E. Carthy, and D.J. Kinahan *Biosensing on the Centrifugal Microfluidic Lab-on-a-Disc Platform*. Processes, 2020. **8**, 1360 DOI: 10.3390/pr8111360.
22. Madadelahi, M., L.F. Acosta-Soto, S. Hosseini, S.O. Martinez-Chapa, and M.J. Madou *Mathematical modeling and computational analysis of centrifugal microfluidic platforms: a review*. Lab on a Chip, 2020. **20**, 1318-1357 DOI: 10.1039/c9lc00775j.
23. Homann, A.R., L. Niebling, S. Zehnle, M. Beutler, L. Delamotte, M.-C. Rothmund, D. Czurratis, K.-D. Beller, R. Zengerle, H. Hoffmann, and N. Paust *A microfluidic cartridge for fast and accurate diagnosis of Mycobacterium tuberculosis infections on standard laboratory equipment*. Lab on a Chip, 2021. DOI: 10.1039/d1lc00035g.

24. *Abaxis*. Available on: https://www.abaxis.com/.
25. Schembri, C.T., V. Ostoich, P.J. Lingane, T.L. Burd, and S.N. Buhl *Portable Simultaneous Multiple Analyte Whole-Blood Analyzer for Point-of-Care Testing*. Clinical Chemistry, 1992. **38**, 1665-1670 DOI: 10.1093/clinchem/38.9.1665.
26. Schembri, C.T., T.L. Burd, A.R. Kopfsill, L.R. Shea, and B. Braynin *Centrifugation and Capillarity Integrated into a Multiple Analyte Whole-Blood Analyzer*. Journal of Automatic Chemistry, 1995. **17**, 99-104 DOI: 10.1155/S1463924695000174.
27. *Gyros Protein Technologies*. Available on: https://www.gyrosproteintechnologies.com/.
28. Shea, M. *ADMET Assays on Tecan's LabCD-ADMET System*. Journal of the Association for Laboratory Automation, 2003. **8**, 74-77 DOI: 10.1016/s1535-5535(04)00260-6.
29. *Biosurfit SA*. Available on: https://www.biosurfit.com/.
30. *Gamera Bioscience Corp. [acquired by Tecan]*.
31. *Radisens Diagnostics*. Available on: www.radisens.com.
32. *LaMotte Chemical Products Co*. Available on: https://www.lamotte.com.
33. *Blusense Diagnostics*. Available on: https://blusense-diagnostics.com/.
34. *Spindiag GmbH*. Available on: http://www.spindiag.de.
35. *RotaPrep Inc.*; Accessed: 19/04/2021; Available on: https://rotaprep.com/.
36. Ducrée, J. *Efficient Development of Integrated Lab-On-A-Chip Systems Featuring Operational Robustness and Manufacturability*. Micromachines, 2019. **10**, DOI: 10.3390/mi10120886.
37. Ducrée, J. *Systematic review of centrifugal valving based on digital twin modelling towards highly integrated Lab-on-a-Disc systems*. Nature Microsystems & Nanoengineering, 2021.
38. Abi-Samra, K., R. Hanson, M. Madou, and R.A. Gorkin *Infrared controlled waxes for liquid handling and storage on a CD-microfluidic platform*. Lab on a Chip, 2011. **11**, 723-726 DOI: 10.1039/c0lc00160k.
39. Kong, L.X., K. Parate, K. Abi-Samra, and M. Madou *Multifunctional wax valves for liquid handling and incubation on a microfluidic CD*. Microfluidics and Nanofluidics, 2015. **18**, 1031-1037 DOI: 10.1007/s10404-014-1492-x.
40. García-Cordero, J.L., D. Kurzbuch, F. Benito-Lopez, D. Diamond, L.P. Lee, and A.J. Ricco *Optically addressable single-use microfluidic valves by laser printer lithography*. Lab on a Chip, 2010. **10**, 2680-7 DOI: 10.1039/c004980h.
41. Stumpf, F., F. Schwemmer, T. Hutzenlaub, D. Baumann, O. Strohmeier, G. Dingemanns, G. Simons, C. Sager, L. Plobner, F. von Stetten, R. Zengerle, and D. Mark *LabDisk with complete reagent prestorage for sample-to-answer nucleic acid based detection of respiratory pathogens verified with influenza A H3N2 virus*. Lab on a Chip, 2016. **16**, 199-207 DOI: 10.1039/c5lc00871a.
42. Delgado, S.M., D.J. Kinahan, F.S. Sandoval, L.A. Julius, N.A. Kilcawley, J. Ducrée, and D. Mager *Fully automated chemiluminescence detection using an electrified-Lab-on-a-Disc (eLoaD) platform*. Lab on a Chip, 2016. **16**, 4002-4011 DOI: 10.1039/c6lc00973e.
43. Torres Delgado, S.M., D.J. Kinahan, L.A. Nirupa Julius, A. Mallette, D.S. Ardila, R. Mishra, C.M. Miyazaki, J.G. Korvink, J. Ducrée, and D. Mager *Wirelessly powered and remotely controlled valve-array for highly multiplexed analytical assay automation on a centrifugal microfluidic platform*. Biosensors and Bioelectronics, 2018. **109**, 214-223 DOI: 10.1016/j.bios.2018.03.012.
44. Gorkin, R., 3rd, C.E. Nwankire, J. Gaughran, X. Zhang, G.G. Donohoe, M. Rook, R. O'Kennedy, and J. Ducrée *Centrifugo-pneumatic valving utilizing dissolvable films*. Lab on a Chip, 2012. **12**, 2894-902 DOI: 10.1039/c2lc20973j.

45. Godino, N., R. Gorkin, 3rd, A.V. Linares, R. Burger, and J. Ducrée *Comprehensive integration of homogeneous bioassays via centrifugo-pneumatic cascading*. Lab on a Chip, 2013. **13**, 685-94 DOI: 10.1039/c2lc40722a.
46. Kinahan, D.J., P.L. Early, A. Vembadi, E. MacNamara, N.A. Kilcawley, T. Glennon, D. Diamond, D. Brabazon, and J. Ducree *Xurography actuated valving for centrifugal flow control*. Lab on a Chip, 2016. **16**, 3454-9 DOI: 10.1039/c6lc00568c.
47. Mishra, R., J. Gaughran, D. Kinahan, and J. Ducrée *Functional Membranes for Enhanced Rotational Flow Control on Centrifugal Microfluidic Platforms*. Reference Module in Materials Science and Materials Engineering, 2017. DOI: 10.1016/b978-0-12-803581-8.04041-8.
48. Kinahan, D.J., S.M. Kearney, N. Dimov, M.T. Glynn, and J. Ducrée *Event-triggered logical flow control for comprehensive process integration of multi-step assays on centrifugal microfluidic platforms*. Lab on a Chip, 2014. **14**, 2249-58 DOI: 10.1039/c4lc00380b.
49. Kinahan, D.J., K. McConville, B. Henderson, M. McCaul, E. McNamara, D. Diamond, and J. Ducrée, *Digital pulse actuated flow control on a centrifugal disc towards multiparameter water quality monitoring*, in *20th International Conference on Miniaturized Systems for Chemistry and Life Sciences (μTAS 2016)*, N. Pamme and J. Ducrée, Editors. 2016, CBMS: Dublin, Ireland. p. 871-872
50. Kinahan, D.J., S.M. Kearney, N.A. Kilcawley, P.L. Early, M.T. Glynn, and J. Ducrée *Density-Gradient Mediated Band Extraction of Leukocytes from Whole Blood Using Centrifugo-Pneumatic Siphon Valving on Centrifugal Microfluidic Discs*. PLOS ONE, 2016. **11**, e0155545 DOI: 10.1371/journal.pone.0155545.
51. Kinahan, D.J., M. Renou, D. Kurzbuch, N.A. Kilcawley, E. Bailey, M.T. Glynn, C. McDonagh, and J. Ducrée *Baking Powder Actuated Centrifugo-Pneumatic Valving for Automation of Multi-Step Bioassays*. Micromachines, 2016. **7**, DOI: 10.3390/mi7100175.
52. Mishra, R., G. Reilly, M. Agnew, A. Garvey, C. Rogers, E. Andrade, H. Ma, S. Fitzgerald, J. Zapatero, R. O'Kennedy, and J. Ducrée, *Laser-Actuated Centrifugo-Pneumatic Flow Control Towards 'Sample-to-Answer' Integrated Detection of Multi-Marker Panels at the Point-of-Care*, in *2018 IEEE Micro Electro Mechanical Systems (MEMS)*. 2018: Belfast, Northern Ireland. p. 1185-1188 DOI: 10.1109/MEMSYS.2018.8346774.
53. Ducrée, J., S. Haeberle, T. Brenner, T. Glatzel, and R. Zengerle *Patterning of flow and mixing in rotating radial microchannels*. Microfluidics and Nanofluidics, 2006. **2**, 97-105 DOI: 10.1007/s10404-005-0049-4.
54. Ducrée, J., T. Brenner, S. Haeberle, T. Glatzel, and R. Zengerle *Multilamination of flows in planar networks of rotating microchannels*. Microfluidics and Nanofluidics, 2006. **2**, 78-84 DOI: 10.1007/s10404-005-0056-5.
55. Brenner, T., T. Glatzel, R. Zengerle, and J. Ducrée *Frequency-dependent transversal flow control in centrifugal microfluidics*. Lab on a Chip, 2005. **5**, 146-50 DOI: 10.1039/b406699e.
56. Clime, L., J. Daoud, D. Brassard, L. Malic, M. Geissler, and T. Veres *Active pumping and control of flows in centrifugal microfluidics*. Microfluidics and Nanofluidics, 2019. **23**, DOI: 10.1007/s10404-019-2198-x.
57. Grumann, M., A. Geipel, L. Riegger, R. Zengerle, and J. Ducrée *Batch-mode mixing on centrifugal microfluidic platforms*. Lab on a Chip, 2005. **5**, 1184-1184 DOI: 10.1039/b418253g.
58. Siegrist, J., R. Gorkin, M. Bastien, G. Stewart, R. Peytavi, H. Kido, M. Bergeron, and M. Madou *Validation of a centrifugal microfluidic sample lysis and homogenization platform for nucleic acid extraction with clinical samples*. Lab on a Chip, 2010. **10**, 363-371 DOI: 10.1039/b913219h.
59. Zehnle, S., F. Schwemmer, R. Bergmann, F. von Stetten, R. Zengerle, and N. Paust *Pneumatic siphon valving and switching in centrifugal microfluidics controlled by rotational frequency or rotational acceleration*. Microfluidics and Nanofluidics, 2015. **19**, 1259-1269 DOI: 10.1007/s10404-015-1634-9.

60. Gaughran, J., D. Boyle, J. Murphy, R. Kelly, and J. Ducrée *Phase-selective graphene oxide membranes for advanced microfluidic flow control*. Microsystems and Nanoengineering, 2016. **2**, 16008 DOI: 10.1038/micronano.2016.8.

61. Kinahan, D.J., S.M. Kearney, O.P. Faneuil, M.T. Glynn, N. Dimov, and J. Ducrée *Paper imbibition for timing of multi-step liquid handling protocols on event-triggered centrifugal microfluidic lab-on-a-disc platforms*. RSC Advances, 2015. **5**, 1818-1826 DOI: 10.1039/c4ra14887h.

62. Godino, N., E. Vereshchagina, R. Gorkin, and J. Ducrée *Centrifugal automation of a triglyceride bioassay on a low-cost hybrid paper-polymer device*. Microfluidics and Nanofluidics, 2014. **16**, 895-905 DOI: 10.1007/s10404-013-1283-9.

63. Delgado, S.M.T., D.J. Kinahan, L.A.N. Julius, A. Mallette, D.S. Ardila, R. Mishra, C.M. Miyazaki, J.G. Korvink, J. Ducrée, and D. Mager *Wirelessly powered and remotely controlled valve-array for highly multiplexed analytical assay automation on a centrifugal microfluidic platform*. Biosensors & Bioelectronics, 2018. **109**, 214-223 DOI: 10.1016/j.bios.2018.03.012.

64. Ducrée, J., M. Etzrodt, S. Bartling, R. Walshe, T. Harrington, N. Wittek, S. Posth, K. Wittek, A. Ionita, W. Prinz, and J. Lawton *Unchaining Collective Intelligence for Science, Research and Technology Development by Blockchain-Boosted Community Participation*. Frontiers in Blockchain, 2020. DOI: 10.3389/fbloc.2021.631648.

65. Ducrée, J. *Research – A blockchain of knowledge?* Blockchain: Research and Applications, 2020. **1**, 100005 DOI: 10.1016/j.bcra.2020.100005.

66. Ducrée, J., M. Gravitt, R. Walshe, S. Bartling, M. Etzrodt, and T. Harrington *Open Platform Concept for Blockchain-Enabled Crowdsourcing of Technology Development and Supply Chains*. Frontiers in Blockchain, 2020. **3**, 386525 DOI: 10.3389/fbloc.2020.586525.

67. Ducrée, J., M. Etzrodt, B. Gordijn, M. Gravitt, S. Bartling, R. Walshe, and T. Harrington *Blockchain for Organising Effective Grass-Roots Actions on a Global Commons: Saving The Planet*. Frontiers in Blockchain, 2020. **3**, 33 DOI: 10.3389/fbloc.2020.00033.